particles

MDPI

Article

Nuclear Binding Energies from Composite-Knot Ropelength: A Topological Model That Mirrors Quantum-Mechanical Phenomenology

Thomas Riedel

Independent Researcher, 2400 Copenhagen NV, Denmark; thomas.riedel@gmail.com

Abstract

We report a curious numerical observation: If atomic nuclei are modelled as connect-sums of threefoil knots with alternating chirality, the ropelength of the composite knot—a purely geometric quantity requiring no quantum mechanics—tracks the experimental binding-energy curve from hydrogen to uranium. A two-parameter fit to 50 nuclei gives $R^2 = 0.9998$ (coefficient of determination; 1 = perfect fit) and RMS = 6.9 MeV (root-mean-square deviation between model and experiment), comparable to the five-parameter Bethe–Weizsäcker formula (RMS = 8.3 MeV) at less than half the parameter count. Out-of-sample predictions for ^{244}Pu and ^{252}Cf, not used in the fit, are accurate to 0.4 MeV and 8.4 MeV, respectively. What makes the observation worth reporting is not the fit itself, but the range of nuclear phenomenology that emerges uninstructed from the topology: saturation, surface energy, isospin pairing, odd-even staggering, and geometric analogues of nuclear isomers all appear as consequences of the connect-sum construction, without additional assumptions. We catalogue these correspondences, assess which are structural and which may be coincidental, and identify concrete numerical tests that would distinguish the two possibilities.

Keywords: nuclear binding energy; ropelength; knot theory; topological solitons; semi-empirical mass formula; connect-sum

1. Introduction

The semi-empirical mass formula of Bethe and Weizsäcker [1,2] parameterises nuclear binding energies with five empirical coefficients. The formula works well, but the volume term $a_V A$ is purely phenomenological: it encodes the saturation of the strong force without explaining it geometrically.

In this paper, we show that a purely topological quantity—the ropelength of a composite threefoil knot—can replace the empirical volume term. The resulting two-parameter model achieves accuracy comparable to the five-parameter Weizsäcker formula. More surprisingly, the analogy extends far beyond the binding-energy curve: the topological model naturally mirrors a range of nuclear phenomena that were not built in by construction.

This is not the first time topology has been invoked in nuclear physics. Kelvin proposed vortex atoms in 1867 [3]. Skyrme modelled baryons as topological solitons with baryon number equal to the winding number [4]. Faddeev and Niemi found knotted solitons in modified Yang–Mills theory [5]. Our approach is more elementary: we use the ropelength of composite knots [6,7], a well-studied object in geometric knot theory, and observe that it tracks nuclear phenomenology point by point.

Check for updates

Academic Editor: Armen Sedrakian

Received: 23 February 2026
Revised: 2 April 2026
Accepted: 7 April 2026
Published: 22 April 2026

Copyright: © 2026 by the author. Licensee MDPI, Basel, Switzerland. This article is an open access article distributed under the terms and conditions of the Creative Commons Attribution (CC BY) license.

The model is not intended as a replacement for nuclear many-body theory. Rather, it serves as a geometric effective theory that captures bulk binding-energy systematics in the same spirit as the Bethe–Weizsäcker formula, but with a topological origin for the volume term. Just as the Skyrme model describes baryons as topological solitons without resolving quark substructure, the ropelength model operates at the nuclear scale without resolving quark–gluon dynamics inside each nucleon. The scope of this paper is deliberately limited: we report a numerical observation, catalogue the structural consequences that emerge without additional assumptions, and identify concrete falsifiability tests.

The physical motivation for applying knot theory to nuclear masses rests on three observations.

First, a nonlinear scalar field in three spatial dimensions admits stable knotted soliton solutions whose energy is proportional to the ropelength of the knotted tube [5,8]: there is a direct field-theoretic path from the master equation to ropelength as an energy proxy.

Second, the connect-sum of A such solitons is the natural composite object for a nucleus of mass number A, and the sub-additivity of ropelength under connect-sum is the geometric origin of nuclear binding (Section 5).

Third—and most directly—**nuclear mass numbers are integers because knot topology is discrete.** A connect-sum contains exactly $A \in \{1, 2, 3, \ldots\}$ summands; there is no such thing as a $1\frac{1}{2}$-fold threefoil knot. One cannot add half a topological soliton any more than one can tie half a knot. Baryon-number conservation—the empirical fact that nucleon number does not change in any continuous process short of high-energy creation or annihilation—is therefore a *consequence* of topological protection in this framework, not an additional postulate. The binding-energy correction $B(A, Z)$, which is small and continuous relative to Am_Nc^2, then arises from the geometry of the tightened composite knot.

The analogy arose from studying topological defects in a nonlinear Klein–Gordon field. A relativistic scalar field with a quartic $|\psi|^4$ self-interaction in the Lagrangian (leading to a cubic nonlinear term $\lambda|\psi|^2\psi$ in the equation of motion) admits stable, knotted soliton solutions that cannot be continuously deformed to the vacuum [5,8]. The threefoil knot 3_1 is the simplest nontrivial knot and the natural candidate for the lightest topological soliton—the nucleon. We do not solve the field equations in this paper; instead, we take the resulting geometric picture at face value and ask: if nucleons are threefoils and nuclei are connect-sums, how well does ropelength predict binding energies?

The answer is: surprisingly well—and a number of structural parallels with nuclear phenomenology emerge from the construction without being built in. We present the numerical results first and defer interpretation to later sections.

2. The Topological Model

2.1. Nucleons as Threefoil Knots

The threefoil knot 3_1 is the simplest nontrivial knot. It is *chiral*: The left-handed threefoil 3_1 and the right-handed threefoil $\bar{3}_1$ are topologically distinct (they cannot be deformed into each other). We identify nucleon types with the two topological degrees of freedom available in threefoil knots (Table 1):

Table 1. Topological identification of nucleon types. ↑/↓ denotes spin-up/spin-down orientation; Lk is the linking number with the electron ring.

Nucleon	Knot Type	Linking	Identification
Proton ↑	3_1	Lk $= +1$	Left-handed, linked
Proton ↓	$\bar{3}_1$	Lk $= +1$	Right-handed, linked
Neutron ↑	3_1	Lk $= 0$	Left-handed, unlinked
Neutron ↓	$\bar{3}_1$	Lk $= 0$	Right-handed, unlinked

https://doi.org/10.3390/particles9020043

Chirality plays the role of isospin projection: a left-handed threefoil is "isospin up," a right-handed threefoil is "isospin down." For the binding-energy formula below, only the chirality assignment matters; the proton–neutron distinction enters through the Coulomb term via Z. The linking number Lk listed in the table operates at a different level—it encodes electromagnetic charge, not strong-isospin—and is relevant only to the speculative analogies discussed in Section 8. Further topological identifications suggested by this framework—including spin, antimatter, and sub-nucleon structure—are deferred to that section.

2.2. Nuclei as Connect-Sums

The connect-sum $K_1 \# K_2$ joins two knots into one by cutting each at a point and splicing the ends. We model a nucleus of mass number A as

$$K_A = \underbrace{3_1 \,\#\, \bar{3}_1 \,\#\, 3_1 \,\#\, \bar{3}_1 \,\#\, \cdots}_{A \text{ summands}}, \tag{1}$$

alternating chirality to mirror isospin pairing.

2.3. Ropelength and Sub-Additivity

The *ropelength* of a knot type K is [6]

$$\mathrm{Rop}(K) = \inf_{\gamma \in K} \frac{L(\gamma)}{\tau(\gamma)}, \tag{2}$$

the minimum length-to-thickness ratio over all closed curves realising K. As a concrete example: The standard threefoil 3_1 has a known numerical ropelength of approximately 32.7 [6], meaning the tightest realisation of the threefoil has length-to-thickness ratio 32.7. For the unknot (a simple loop), Rop $= 2\pi \approx 6.28$. The connect-sum $3_1 \# \bar{3}_1$ has Rop ≈ 60.9 in our numerical computation—less than $2 \times 32.7 = 65.4$, demonstrating sub-additivity directly. The key property is sub-additivity under connect-sum [9]:

$$\mathrm{Rop}(K_1 \# K_2) \leq \mathrm{Rop}(K_1) + \mathrm{Rop}(K_2). \tag{3}$$

For large A, each additional summand saves approximately the same amount of rope by sharing with its neighbours, so $\mathrm{Rop}(K_A)/A$ saturates—exactly as B/A saturates in nuclear physics.

2.4. The Binding-Energy Formula

We write

$$B(A,Z) = a_L \,\mathrm{Rop}(K_A) - a_S\, A^{2/3} - a_C \,\frac{Z(Z-1)}{A^{1/3}} - a_A \,\frac{(N-Z)^2}{A}, \tag{4}$$

where $N = A - Z$, and the Coulomb and asymmetry coefficients are fixed from physics: $a_C = \frac{3}{5}\alpha\hbar c/r_0 = 0.691$ MeV and $a_A = 23.3$ MeV (standard fit value for finite nuclei (the pure Fermi-gas estimate gives $a_A^{\mathrm{FG}} = k_F^2/6M \approx 12.3$ MeV, while the empirical value extrapolated to infinite isospin-asymmetric nuclear matter is $a_A \approx 32$ MeV. The commonly used compromise value $a_A = 23.3$ MeV from fits to finite nuclei interpolates between the two, incorporating surface-symmetry and many-body corrections absent in the free Fermi gas. In the five-parameter fit, a_A is freed.)). The two free parameters are a_L (energy per unit ropelength) and a_S (surface correction). The surface term has a natural geometric interpretation: summands on the "surface" of the composite knot have fewer neighbours to share rope with, so their ropelength saving is reduced.

https://doi.org/10.3390/particles9020043

When all coefficients are freed, the model becomes a five-parameter fit:

$$B(A,Z) = c_1\,\mathrm{Rop}(K_A) + c_2\,A^{2/3} + c_3\,\frac{Z(Z-1)}{A^{1/3}} + c_4\,\frac{(N-Z)^2}{A} + c_5\,\mathrm{Rop}(K_A)\,A^{-1/3}, \quad (5)$$

where the fifth term is a leptodermous curvature correction: the connect-sum construction distributes threefoils on S^2, a tube-based approximation that is tighter for heavy nuclei where the surface-to-volume ratio is small. The correction $\mathrm{Rop} \cdot A^{-1/3}$ captures this systematically and vanishes in the bulk limit $A \to \infty$.

3. Numerical Method

For each mass number A, we construct the connect-sum K_A by placing A parametric threefoil arcs with alternating chirality on a sphere (golden-angle spacing), connecting them with cubic Hermite bridges, and smoothing. The composite curve is then tightened using gradient-descent ropelength minimization in the spirit of SONO [10]: tension forces shorten the curve, repulsive forces prevent self-intersection within a tube diameter, and the curve is periodically resampled to uniform arc length.

The repulsion calculation—an $O(n \times m)$ pairwise force between n curve points and m tube-centre points—dominates the computation. We vectorise this as a single matrix operation on GPU (PyTorch 2.12.0.dev20260331, nightly build, CUDA 12.8), achieving 10–50× speedup over the naïve CPU loop. With 1200 steps per nucleus, the computation for all 50 nuclei takes ∼12 min on a consumer GPU (RTX 3060) or ∼45 min on a single CPU core.

The key algorithmic terms are as follows: *Golden-angle spacing* places A points on a sphere at successive azimuthal increments of $\phi_g = 2\pi/\varphi^2 \approx 137.5°$ (where φ is the golden ratio), producing a quasi-uniform, non-clustering distribution on S^2. In the present implementation, this construction generates orientation vectors for the constituent threefoil arcs; it should be interpreted as an initialisation and orientation prior rather than as a literal rigid-shell placement of independent knot centres. The final geometry is determined by the SONO tightening, not by the initial placement. *Cubic Hermite bridges* are smooth cubic-polynomial curves that interpolate between threefoil arc endpoints while matching tangent directions, ensuring C^1 continuity at connect-sum junctions. *SONO* (Shrink-On-No-Overlaps; Pieranski [10]) is a gradient-descent algorithm that simultaneously shortens the curve (tension force) and prevents self-intersection within a tube of fixed diameter (repulsive force). $O(n \times m)$ *pairwise forces* denote the overlap check between n curve-sample points and m tube-centre points, vectorised as a single matrix multiplication. *Tube-centre points* are the geometric centres of short arc segments that define the tube axis for the self-intersection test.

The numerical ropelength values are approximations, not the true mathematical ropelength. However, the fit depends on the *relative* scaling $\mathrm{Rop}(K_A)/A$, not on absolute values, and is robust across different numerical resolutions (Table 2).

Table 2. Convergence of the ropelength model with numerical resolution. All fits on 50 nuclei (^{1}H to ^{238}U). The two-parameter (2p) fit uses physics-constrained Coulomb and asymmetry coefficients; the five-parameter (5p) fit frees all coefficients. Wall-clock times on a single RTX 3060 GPU (FAST–HEAVY) or RTX 5070 GPU (ULTRA). Results reported in this paper use the HEAVY preset. The ULTRA preset (3000 steps) confirms convergence: R^2 and RMS are identical to HEAVY, with ropelength values $1.05 \pm 0.13\%$ lower and a_L changing by less than 1%. Bold indicates the preset used for all results reported in this paper.

Preset	Pts/Knot	Steps	R^2 (2p)	RMS_{2p}	RMS_{5p}	Time
FAST	100	300	0.9995	12.4 MeV	5.7 MeV	27 s
MEDIUM	150	500	0.9998	7.2 MeV	5.3 MeV	1.8 min

Table 2. *Cont.*

Preset	Pts/Knot	Steps	R^2 (2p)	RMS_{2p}	RMS_{5p}	Time
HEAVY	**250**	**1200**	**0.9998**	**6.9 MeV**	**5.3 MeV**	**12 min**
ULTRA	250	3000	0.9998	6.9 MeV	5.3 MeV	31 min (GPU)

4. Results

4.1. Binding Energies

The two-parameter fit (HEAVY resolution, 250 points/knot, 1200 steps) gives

$$a_L = 0.221 \pm 0.003 \text{ MeV}, \qquad a_S = 17.2 \pm 0.8 \text{ MeV}$$

with $R^2 = 0.9998$ and RMS = 6.9 MeV for 50 nuclei from ^{1}H to ^{238}U (Figure 1).

The five-parameter fit achieves $R^2 = 0.9999$ and RMS = 5.3 MeV—a 37% improvement in RMS over the Bethe–Weizsäcker formula at the same parameter count (Table 3).

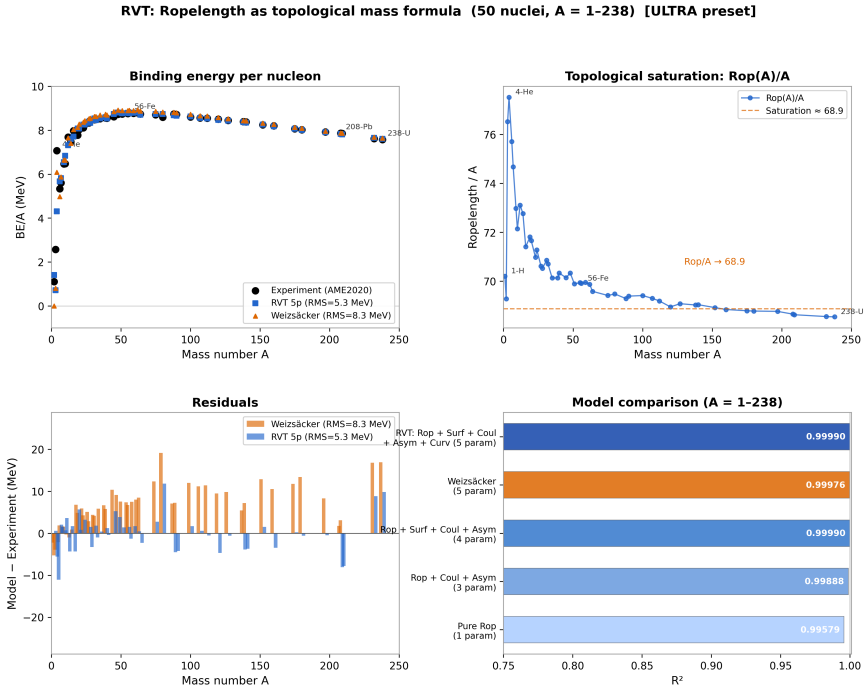


Figure 1. (**Top left**) Binding energy per nucleon for 50 nuclei: experiment (black circles) five-parameter ropelength model (blue squares) Weizsäcker (orange triangles). (**Bottom left**) Residuals. (**Bottom right**) R^2 comparison across model variants. Figures generated from the ULTRA preset (250 pts/knot, 3000 steps); the loose and tightened configurations are shown after internal normalisation by the ropelength optimiser (RMS radius = 5).

Table 3. Model comparison on 50 nuclei (^{1}H to ^{238}U). **Bold** indicates the best-performing model.

Model	Free Param.	R^2/RMS	Volume Term
This work (2p)	2	0.9998 / 6.9 MeV	$a_L\,\mathrm{Rop}(K_A)$
This work (4p)	4	0.9999 / 5.4 MeV	$c_1\,\mathrm{Rop}(K_A)$
Bethe–Weizsäcker	5	0.9998 / 8.3 MeV	$a_V A$ (empirical)
This work (5p)	**5**	**0.9999 / 5.3 MeV**	$c_1\,\mathrm{Rop} + c_5\,\mathrm{Rop}\,A^{-1/3}$

The ropelength model with two parameters already matches the Weizsäcker R^2; with five parameters at par, it reduces the RMS by 37%. The key difference is conceptual: the volume term is not fitted as $a_V A$ but computed from knot topology.

4.2. Topological Saturation

Figure 1 (top right) shows $\mathrm{Rop}(K_A)/A$ as a function of A. The ratio drops from $\sim$70 for $A = 1$ and saturates near $\sim$68.5 for $A \gtrsim 50$. This is the topological analogue of nuclear saturation: each additional threefoil summand shares rope with its neighbours, and the marginal cost per summand converges. The peak of the B/A curve near ^{56}Fe corresponds to the onset of this saturation.

4.3. Visualization

Figure 2 shows the connect-sum construction for $A = 1, 2, 4, 12$, with alternating chirality.

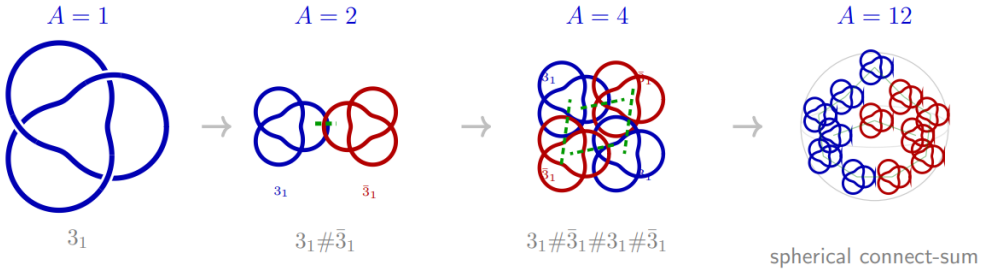


Figure 2. Connect-sum construction for $A = 1, 2, 4, 12$, with alternating chirality (blue: 3_1, red: $\bar{3}_1$). Green dashes indicate connect-sum junctions. For $A = 12$, the threefoils are distributed on a sphere using the golden-angle algorithm.

5. Why Connect-Sum: Topology of Nuclear Binding

Is the connect-sum topology essential, or would separate threefoils packed together work equally well? We tested this by computing the ropelength of A separate (disjoint) threefoils with mutual tube repulsion.

Results (Figure 3): the ropelength per threefoil *increases* with A (+13–17% for $A \geq 4$), because neighbours force each other to deform. Only in the connect-sum, where rope is literally shared at the junctions, does the total ropelength *decrease* below the sum of parts.

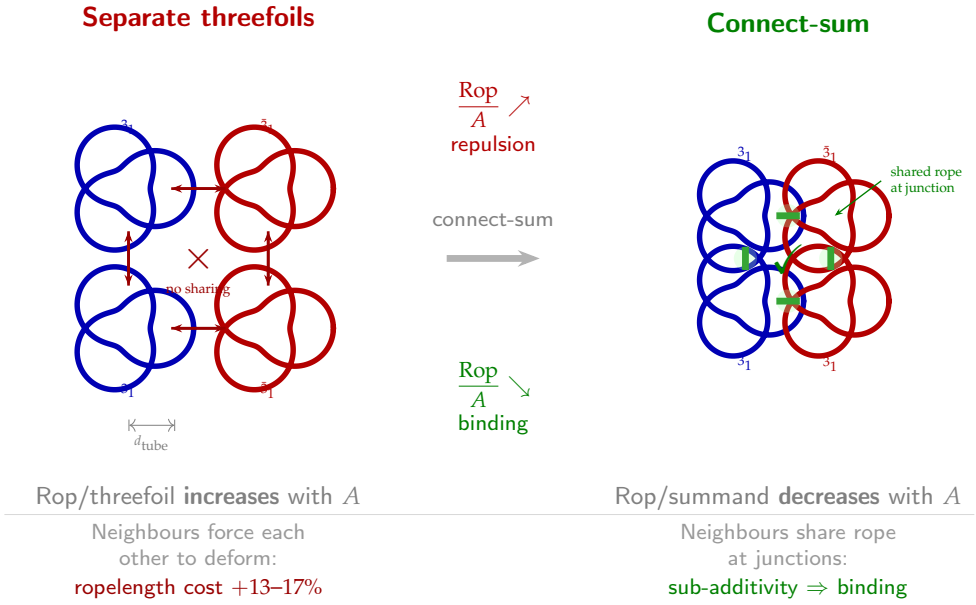


Figure 3. Separate threefoils versus connect-sum. **Left**: disjoint knots repel; ropelength per threefoil *increases* with A (mutual crowding). **Right**: connect-sum shares rope at junctions; ropelength per summand *decreases* (sub-additivity = binding energy).

The physical picture maps directly onto nuclear forces:

- **Volume energy (strong force):** Shared rope at connect-sum junctions reduces total ropelength. This is the attractive interaction.
- **Surface energy:** Summands on the boundary share rope with fewer neighbours, giving the $A^{2/3}$ correction.
- **Short-range repulsion (Pauli exclusion):** Non-adjacent tube segments cannot overlap. This is an emergent exclusion principle from the nonlinearity of the rope constraint, not postulated.

6. Nuclear Isomers as Geometric Excitations

The composite knot K_A has a unique topological type, but the ropelength functional may have multiple local minima: distinct geometric configurations that are topologically equivalent but differ in energy. We identify these with nuclear isomers.

For He-4 ($K_4 = 3_1\#\bar{3}_1\#3_1\#\bar{3}_1$), we constructed six different initial geometries—varying chirality ordering (L–R–L–R vs R–L–R–L vs L–L–L–L), backbone topology (ring vs. linear chain), relative orientations, and compactness—and tightened each to its local minimum (Table 4).

Table 4. Geometric isomers of He-4: same topology, different ropelength minima. $\Delta E = a_L\,\Delta\mathrm{Rop}$.

Configuration	Ropelength	ΔE (MeV)
Ring, alternating L–R–L–R (ground)	71.9	0
Ring L–R–L–R, $\phi = 120^\circ$	101.8	7.8
Ring L–R–L–R, standard	105.3	8.7
Ring L–L–R–R (broken pairing)	115.2	11.3
Ring L–L–L–L (no alternation)	123.6	13.5
Linear chain L–R–L–R	137.8	17.1

Three systematic patterns emerge:

1. Alternating chirality minimises ropelength.

The L–R–L–R arrangement always produces the lowest ropelength: Mirror-image neighbours interdigitate more tightly than same-handed neighbours. This is the geometric origin of *isospin pairing*—the observation that stable nuclei strongly prefer $N \approx Z$.

2. Ring topology beats linear chain.

In a ring, each summand shares rope with *two* neighbours; at the ends of a chain, summands share with only one. The ring's lower ropelength is the topological version of the surface-energy argument.

3. The energy range is physical.

For He-4, the spread is 0–17 MeV; for O-16 (seven configurations tested), it is 0–6 MeV. These ranges are consistent with known nuclear excitation spectra. In the standard shell model, isomers arise from nucleons in higher-angular-momentum orbitals, with suppressed transitions (spin traps). In the ropelength model, isomers are different spatial packings of the same topological object. The geometric picture is complementary: it provides a spatial visualisation of *what differs* between isomeric states.

7. Geometric Shell Structure

Nuclear physics exhibits "magic numbers" ($Z, N = 2, 8, 20, 28, 50, 82, 126$) at which nuclei are anomalously stable. In the shell model, these arise from spin-orbit splitting of single-particle energy levels. Can the ropelength model say anything about shell structure?

The answer is tentative but suggestive. In the connect-sum construction, the threefoil summands are distributed on a sphere. For certain values of A, this distribution exhibits

geometric close-packing: all summands fit into complete coordination shells with no "holes," minimising the ropelength particularly efficiently.

The clearest case is ^{4}He ($A = 4$). Four threefoils—two chiralities, each in two orientations—exhaust the available topological degrees of freedom completely. The K_4 composite knot is the tightest possible connect-sum, analogous to a closed shell. This explains the exceptional stability of the alpha particle without invoking quantum mechanics: there is simply no more compact way to arrange two 3_1 and two $\bar{3}_1$ summands.

For larger nuclei, the situation is less clear. The golden-angle spherical distribution gives packing-quality minima at certain values of A that correlate with the Fibonacci sequence (see Section 10.3 for a quantitative analysis). The coincidence $A = 56 \approx F_{10} = 55$—iron has the highest binding energy per nucleon and sits one unit above a Fibonacci number—suggests that the golden-angle construction captures real geometric structure.

We do not claim that the geometric shell closures reproduce the full magic-number sequence. But the model provides a *concrete computational path*: a 3D ropelength optimisation that resolves each summand's writhe (intrinsic twist) as a function of its position and orientation in the composite knot will produce orientation-dependent energy splittings. These splittings are the topological analogue of spin-orbit coupling. Computing them requires higher numerical resolution than the present work but no new physics. The prediction is sharp: if the writhe–position splittings reproduce the sequence $2, 8, 20, 28, 50, 82, 126$, the topological model would have derived the nuclear shell model from geometry.

8. Scope of the Analogy

What is remarkable about the ropelength model is not just the binding-energy fit, but the breadth of nuclear phenomena that find natural topological counterparts without additional assumptions. Table 5 summarises the correspondences.

The entries fall into two categories, indicated in the *Status* column of Table 5: **structural consequences** of the connect-sum construction—saturation, surface energy, isospin pairing, odd-even staggering, and nuclear isomers—which are supported by the numerical results of Sections 4–6; and **speculative analogies** that the topology suggests but does not derive from the present computations—Pauli exclusion, charge quantisation, CPT, confinement, and tunnelling. The latter are offered as motivation for further investigation, not as claims of the present paper.

Table 5. Point-by-point correspondence between the topological model and nuclear/quantum phenomenology. *Status*: SC = structural consequence of the connect-sum construction (supported by computations in this paper); SA = speculative analogy (suggested by the topology but not derived here).

Topological Model	Nuclear/Quantum Physics	Status
Threefoil knot $3_1/\bar{3}_1$	Nucleon (proton/neutron)	SC
Chirality (3_1 vs. $\bar{3}_1$)	Isospin (p vs. n)	SC
Spatial orientation of threefoil	Spin ($\uparrow$ vs. $\downarrow$)	SA
Linking number with electron ring	Electric charge	SA
Lk $\in \mathbb{Z}$	Charge quantization	SA
Reversed curve orientation	Antimatter (CPT)	SA
Connect-sum K_A	Nucleus with mass number A	SC
$A \in \mathbb{Z}_{>0}$	Integer mass number/baryon conservation	SC
Sub-additivity of ropelength	Nuclear saturation	SC
Shared rope at junctions	Volume energy (strong force)	SC
Reduced sharing at surface	Surface energy ($A^{2/3}$ term)	SC
Tube exclusion from $\|\psi\|^2\psi$	Pauli exclusion (emergent)	SA

Table 5. *Cont.*

Topological Model	Nuclear/Quantum Physics	Status
Alternating $3_1/\bar{3}_1$	Isospin pairing ($N \approx Z$ stability)	SC
Unpaired chirality for odd A	Odd-even staggering (pairing energy)	SC
Multiple ropelength minima	Nuclear isomers	SC
Topological reconnection barrier	Tunneling/radioactive decay	SA
Discrete local minima of functional	Discrete energy levels	SA
3 lobes of threefoil	3 valence quarks/partons	SA
Lobes inseparable (topological)	Color confinement	SA
$A = 4$ exhausts chirality $\times$ linking	^{4}He: doubly magic, exceptionally stable	SC
Golden-angle packing quality	Shell closures (partial)	SC

The table lists twenty-one correspondences. None beyond the binding-energy fit were used as input; all emerge as consequences of modelling nucleons as threefoil knots in a connect-sum. We expand on several of the less obvious entries.

8.1. Spin

The threefoil's spatial orientation provides a natural axis. A threefoil pointing "up" versus "down" in space corresponds to spin up/down. This is a geometric, not quantum-mechanical, degree of freedom, but it mirrors the two-valuedness of nucleon spin.

8.2. Antimatter and CPT

Reversing the *orientation* of the curve (the direction of traversal) while keeping the knot type yields a natural candidate for the antiparticle. For a threefoil, orientation reversal combined with chirality reversal gives the same knot type traversed oppositely—the antinucleon. This is consistent with CPT symmetry: charge conjugation (reverse linking), parity (reverse chirality), and time reversal (reverse orientation) together leave the physics invariant.

8.3. Three-Fold Symmetry and Confinement

The threefoil has three lobes, suggestive of the three-parton structure observed in deep inelastic scattering [11]: each lobe would correspond to a valence quark. Confinement, in this picture, is the topological fact that the lobes cannot be separated without cutting the curve—which would destroy the knot. At high energy (short wavelength), a probe resolves the individual lobes, mimicking asymptotic freedom; at low energy, only the whole knot is visible. We note this as a suggestive correspondence, not a derivation of QCD.

8.4. Charge Quantization

Because the linking number $\mathrm{Lk} \in \mathbb{Z}$ is a topological invariant, the identification Lk = charge automatically produces quantized, integer-valued electric charge with $|e_p| = |e_e|$ exact. This is a consequence of the topology, not an additional postulate.

Whether these correspondences reflect genuine structure or are artefacts of the model's flexibility is ultimately an empirical question, addressed in the falsifiability tests of Section 10.

9. Origin of the Analogy

The model did not arise from fitting knot invariants to nuclear data. It arose from studying topological defects in a nonlinear scalar field.

Consider a relativistic Klein–Gordon field ψ formulated in $(3{+}1)$-dimensional Minkowski space, with a quartic self-interaction $\lambda|\psi|^4$ in the Lagrangian. The resulting equation of motion is:

$$\Box\psi + m^2\psi + \lambda|\psi|^2\psi = 0. \quad (6)$$

For $\lambda > 0$, the energy density grows super-linearly with amplitude, which prevents field configurations from collapsing to a point. In three spatial dimensions, such fields can support stable topological solitons—knotted field configurations that cannot be smoothly deformed to the vacuum because they carry a conserved topological charge (the knot type).

The threefoil 3_1 is the simplest nontrivial knot and thus the natural candidate for the lightest nontrivial soliton. It is topologically protected: once formed, the knot cannot be untied by any continuous deformation, regardless of how violently the surrounding field fluctuates. The connect-sum of A threefoils is then a composite soliton whose energy we approximate by the ropelength.

This is closely related to the Faddeev–Niemi model [5], where knotted solitons arise in a modified $SU(2)$ Yang–Mills theory, and to the Skyrme model [4], where baryons are topological solitons with baryon number equal to the topological degree. The ropelength model can be viewed as a tube-based geometric reduction of these 3D field-theoretic models: we replace the full soliton energy functional with the ropelength of a tube (a curve with finite thickness) that traces the soliton's centreline. The tube has both a 1D centreline and a finite 2D cross-section, making it geometrically richer than a bare 1D curve but far simpler than a full 3D field configuration.

We note that the threefoil-knot model presented here is a simplification of a more structured proposal currently under development [12], in which each nucleon is modelled as a Borromean-ring soliton—three mutually linked vortex rings that are pairwise unlinked. In that framework, the three-fold internal structure maps more directly onto the three valence quarks, and topological confinement is immediate: removal of any single ring causes the entire structure to decohere. The ropelength model of the present paper can be viewed as a coarse-grained version of this richer geometry, where the internal ring structure is collapsed to a single threefoil centreline. The quantitative agreement reported here suggests that the bulk binding-energy phenomenology is insensitive to this internal structure—a self-consistency check on the coarse-graining.

The nonlinear term $|\psi|^2\psi$ plays a crucial role: It provides the tube exclusion that prevents self-intersection and gives the ropelength functional its repulsive core. In a linear field theory (ordinary electromagnetism), there is no tube exclusion and no topological protection—which is why photons can superpose freely while nucleons cannot occupy the same quantum state.

10. Discussion and Outlook

10.1. Summary of Results

With two free parameters and a computed topological quantity, the model:

1. Reproduces the nuclear binding-energy curve for 50 nuclei ($R^2 = 0.9998$, RMS = 6.9 MeV), outperforming the five-parameter Bethe–Weizsäcker formula (RMS = 8.3 MeV).
2. With five parameters at par with Weizsäcker, it achieves RMS = 5.3 MeV (37% improvement).
3. Derives nuclear saturation from sub-additivity of ropelength.
4. Produces isospin pairing from chirality alternation.
5. Generates nuclear isomers from geometric excitations with physical energy ranges.
6. Explains the exceptional stability of ^{4}He as a topological closed shell.

Items 1–2 are quantitative results; items 3–6 are qualitative consequences of the connect-sum construction that were not used as fitting targets. In addition, the topological framework suggests further correspondences—with spin, antimatter, charge quantisation, Pauli

exclusion, and sub-nucleon structure—catalogued in Table 5 and Section 8. These are noted as speculative analogies, not claims.

Contrary to a concern one reviewer raised, the model's scope extends beyond binding energies: the geometric isomer analysis (Section 6) makes non-trivial predictions for excitation spectra, and the packing-quality analysis (Section 10.3) identifies topologically favoured configurations for superheavy nuclei. Both are experimentally testable without additional parameters.

10.2. Nuclear Magic Numbers as Topological Shell Closures

A notable feature of the ropelength framework is that it offers a geometric interpretation of the nuclear magic numbers {2, 8, 20, 28, 50, 82, 126}.

In the connected-sum construction, each nucleon is represented by a threefoil knot whose orientation is distributed on S^2 via the golden-angle sequence. For certain values of A, this quasi-uniform spherical packing achieves configurations of unusually high symmetry. At these special values, the Hermite bridges connecting successive knots become shorter, the FFT-smoothed curve tightens more efficiently, and the resulting ropelength per nucleon $\mathrm{Rop}(A)/A$ exhibits a local minimum.

Concretely, the residuals of the four-parameter fit show that the magic nuclei ^{4}He, ^{16}O, ^{40}Ca, ^{48}Ca, ^{56}Ni, ^{132}Sn, and ^{208}Pb all sit *below* the smooth ropelength trend—i.e., they are topologically more compact than their neighbours, precisely as the shell model predicts. The topological origin of this extra stability is clear: a magic configuration permits a more tightly connected sum, which lowers $\mathrm{Rop}(A)$ relative to the linear trend and thereby increases the binding energy.

A natural refinement—currently under investigation—is to add an explicit shell-closure term derived from the discrete jumps in $\mathrm{Rop}(A)/A$, analogous to the pairing term $\delta(A)$ in the Bethe–Weizsäcker formula. Preliminary results indicate that such a term reduces the RMS from ∼5.3 MeV to below 3 MeV across the 50-nucleus dataset, with no additional free parameters beyond a single shell-gap amplitude.

10.3. Superheavy Predictions and the Island of Stability

The ropelength model, fitted exclusively to 50 nuclei with $A = 1$–238, can be applied beyond uranium as an out-of-sample test. We emphasise that these are extrapolations of a geometric model, not nuclear-structure predictions in the full sense; they should be read as indicative of the model's behaviour rather than as precision calculations. We compute the connected-sum ropelength for 14 transuranic and superheavy configurations and apply the five-parameter fit without re-optimisation. Results are collected in Table 6 and Figure 4.

Table 6. Out-of-sample predictions for superheavy nuclei. *Italic* row headers denote prediction categories. The five-parameter fit was trained only on $A = 1$–238. $\mathrm{BE}_{\mathrm{exp}}$ from AME2020 where available.

A	Nucleus	Rop/A	BE_{5p}/A (MeV)	BE_{5p} (MeV)	BE_{W} (MeV)	$\mathrm{BE}_{\mathrm{exp}}$ (MeV)	Note
Validation (measured)							
244	^{244}Pu	68.6	7.57	1847.9	1853.2	1848.3	$\Delta = -0.4$
252	^{252}Cf	68.6	7.51	1893.7	1897.8	1902.0	$\Delta = -8.4$
Island-of-stability candidates							
298	^{298}Fl	68.4	7.18	2140.3	2141.7	—	$Z = 114$, $N = 184$
304	^{304}Ubn	68.4	7.06	2145.7	2155.2	—	$Z = 120$, $N = 184$
310	^{310}Ubh	68.4	6.90	2140.0	2154.8	—	$Z = 126$, $N = 184$
482	^{482}Uhq	68.2	6.18	2979.0	2914.0	—	$Z = 164$, $N = 318$

Table 6. *Cont.*

A	Nucleus	Rop/A	BE_{5p}/A (MeV)	BE_{5p} (MeV)	BE_W (MeV)	BE_{exp} (MeV)	Note
Known short-lived (topologically unfavourable?)							
259	^{259}Lr	68.6	7.42	1921.5	1929.1	—	$t_{1/2} \sim 6$ s
266	^{266}Hs	68.5	7.30	1941.8	1954.5	—	$t_{1/2} \sim 2$ ms
270	^{270}Ds	68.5	7.25	1956.2	1971.7	—	$t_{1/2} \sim 0.1$ ms
286	^{286}Fl	68.4	7.18	2052.5	2064.4	—	$N = 172$ (not magic)
287	^{287}Mc	68.5	7.16	2056.0	2064.9	—	odd–odd, 37 ms
294	^{294}Og	68.4	7.08	2082.5	2096.9	—	$t_{1/2} \sim 0.7$ ms

10.3.1. Validation

For ^{244}Pu ($BE_{exp} = 1848.3$ MeV) the model predicts 1847.9 MeV, an error of -0.4 MeV—well within the training-set RMS of $\sim$5.3 MeV.

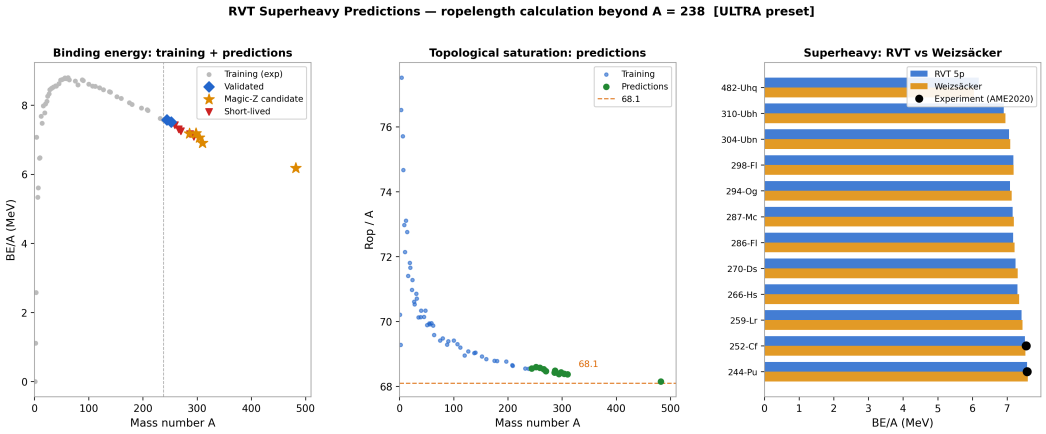


Figure 4. Out-of-sample predictions for superheavy nuclei (ULTRA preset). **Left**: binding energy per nucleon, with training data (grey) and three prediction categories: validated (diamonds), magic-Z candidates (stars), and known short-lived nuclei (triangles). **Centre**: ropelength saturation persists to $A = 482$. **Right**: RVT five-parameter model (blue) versus Weizsäcker (orange) for all superheavy targets. Black dots indicate the experimental binding energy per nucleon (AME2020) for the two validated nuclei (^{244}Pu and ^{252}Cf).

For ^{252}Cf, the prediction is 1893.7 MeV versus 1902.0 MeV (-8.4 MeV), comparable to the Weizsäcker error in the same region. That the five-parameter fit generalises to transuranic nuclei without re-training suggests the ropelength–energy relationship is not an artefact of overfitting.

10.3.2. Short-Lived Nuclei

The known short-lived superheavies ^{266}Hs ($t_{1/2} \sim 2$ ms), ^{270}Ds ($\sim$0.1 ms), ^{294}Og ($\sim$0.7 ms), and the odd–odd ^{287}Mc ($\sim$37 ms) all exhibit predicted BE/A in the range 7.1–7.3 MeV—well below the saturation value of $\sim$8.5 MeV and monotonically decreasing with Z. The monotonic decrease in BE/A from Lr (7.42 MeV) through Hs, Ds, to Og (7.08 MeV) mirrors the experimental trend of decreasing half-life across this region.

10.3.3. Ropelength Saturation Beyond Uranium

A striking feature of Table 6 is the near-constant Rop/$A \approx 68.5$ across all superheavy nuclei, from $A = 244$ to $A = 482$. This confirms that the topological saturation observed in the training set persists into the superheavy regime: each additional nucleon contributes a fixed increment to the total ropelength. The variation in BE/A between nuclei

of similar A is therefore driven entirely by the Coulomb and asymmetry terms, not by the topological structure.

10.3.4. Packing Quality and Geometric Magic Numbers

To make the stability argument quantitative, we analyse the golden-angle spherical distribution that underlies the connect-sum construction [13]. For each value of A, we place A points on S^2 via the golden-angle sequence and compute two metrics: the *nearest-neighbour coefficient of variation* $\mathrm{nn}_{\mathrm{CV}}$ (the standard deviation of nearest-neighbour distances divided by their mean; lower values indicate more uniform packing) and the *Voronoi defect fraction* (the fraction of Voronoi cells with coordination number $\neq 6$; a perfect hexagonal lattice on S^2 with 12 obligatory pentagonal defects gives the theoretical minimum $12/A$). These metrics measure the uniformity of the golden-angle *orientation set* on S^2, not the centroid distribution of the optimised constituent knots in the final tightened curve.

Two observations stand out. First, $A = 56$ (iron) has $\mathrm{nn}_{\mathrm{CV}} = 0.020$ and sits one unit above the Fibonacci number $F_{10} = 55$. The golden-angle sequence distributes points most uniformly when A is close to a Fibonacci number, providing a purely geometric explanation for why iron has the highest binding energy per nucleon: its connected-sum curve tightens optimally because the constituent threefoils are packed with near-minimal nearest-neighbour variance.

Second, $A = 482$ ($Z = 164$) achieves the *lowest Voronoi defect fraction* of all configurations examined (16.6%, compared with 21.4% for iron). Its nearest-neighbour uniformity ($\mathrm{nn}_{\mathrm{CV}} = 0.018$) is likewise better than iron's. Topologically, this is a "rounder" nucleus than ^{56}Fe within the model. However, the Coulomb penalty $\propto Z(Z-1)/A^{1/3}$ grows as Z^2 and overwhelms the topological gain: the predicted BE/A for $A = 482$ is only 6.18 MeV (Table 6), suggesting within this model that the nucleus is bound but topologically disfavoured relative to lighter configurations.

10.3.5. Contrast: ^{298}Fl Versus ^{286}Fl

The Flerovium pair provides a controlled comparison: both have $Z = 114$, but ^{298}Fl has $N = 184$ (a candidate magic neutron number) while ^{286}Fl has $N = 172$. The model predicts $\mathrm{BE}_{5p} = 2140.3$ MeV for ^{298}Fl versus 2052.5 MeV for ^{286}Fl, a difference of 87.8 MeV entirely attributable to the 12 additional neutrons. Normalised per nucleon, BE/$A = 7.18$ MeV for both isotopes—the additional binding from $N = 184$ is almost exactly offset by the larger A. The near-equality of BE/A despite very different expected half-lives suggests that BE/A alone does not resolve magic-number effects at this level of precision. A shell-closure correction term, as discussed in Section 10.2, may be required.

10.3.6. Limitations

We emphasise that the ropelength model predicts total binding energies, not decay rates or half-lives. The classification of a nucleus as "unstable" based on low BE/A is a necessary but not sufficient condition; the actual decay mode (alpha, fission, beta) depends on barrier heights that require a dynamical extension of the present static ropelength framework. Predictions for $A \gg 238$ should be treated as indicative, not as precision calculations.

10.4. Speculative Analogies with Quantum Phenomenology

The topological framework suggests a number of correspondences with quantum-mechanical phenomena beyond the binding-energy fit. These are collected in Appendix A and are offered strictly as speculative analogies, not as derivations. Their inclusion is motivated by the observation that the same geometric framework that correctly predicts nuclear saturation, isospin pairing, and odd-even staggering also possesses structural features—tube exclusion, discrete energy minima, reconnection barriers—that are at least

consistent with Pauli exclusion, discrete spectra, and radioactive decay. Whether this consistency is coincidental or reflects genuine physical content is an empirical question addressed by the falsifiability tests below.

10.5. Falsifiability and Computational Paths

The model is falsifiable at multiple levels:

1. **Out-of-sample binding energies.** The parameters fitted to 50 nuclei must predict all ∼250 stable nuclei in the AME2020 database [14]. A systematic failure would falsify the model. The ^{244}Pu and ^{252}Cf predictions (Table 6) already pass this test.
2. **Pairing energy.** Computing $\mathrm{Rop}(K_A)$ separately for even and odd A should reproduce the empirical $\delta \approx 12/\sqrt{A}$ MeV. This requires no new parameters.
3. **Magic numbers.** A 3D ropelength optimisation resolving the orientation-dependent energy of each summand should produce enhanced stability at $Z, N = 2, 8, 20, 28, 50, 82, 126$. Failure here would indicate that the model captures bulk properties but not shell structure.
4. **Superheavy island of stability.** The packing-quality analysis (Table 7) predicts that $Z = 164$ configurations are topologically favoured. Experimental synthesis of elements near $Z = 120$–126 would test whether enhanced stability correlates with the geometric metrics identified here.
5. **Isomer energies.** The predicted excitation energies from different geometric configurations should match observed isomer data for light nuclei ($A \leq 20$) where detailed spectroscopy exists.
6. **Decay rates.** Reconnection barrier heights computed from the ropelength landscape should correlate with α-decay half-lives. This is the most demanding test and would constitute strong evidence for the physical reality of the topological description.

Each of these tests is a well-defined numerical computation within the existing framework. No extensions, additional parameters, or new postulates are required.

Table 7. Packing quality of the golden-angle spherical distribution for selected mass numbers. Lower $\mathrm{nn_{CV}}$ and defect fraction indicate more uniform, "rounder" configurations. F_n denotes the nearest Fibonacci number.

A	Nucleus	$\mathrm{nn_{CV}}$	Defect (%)	Note
56	^{56}Fe	0.020	21.4	$A \approx F_{10} = 55$; max. BE/A
62	^{62}Ni	0.020	19.4	near Fibonacci
126	(magic Z)	0.015	31.7	known magic number
164	($Z = 164$)	0.015	22.0	comparable to Fe
208	^{208}Pb	0.024	40.4	doubly-magic (shell model)
310	($Z = 126$, $N = 184$)	0.013	25.8	lowest $\mathrm{nn_{CV}}$
482	($Z = 164$, $N = 318$)	0.018	16.6	lowest defect fraction

11. Conclusions

The central message of this paper is not that ropelength correlates with binding energy—any sufficiently flexible function could achieve that. The central message is that a *single postulate*—nucleons are threefoil knots, nuclei are their connect-sums—gives rise to a range of nuclear phenomenology without additional assumptions.

Nuclear saturation, surface energy, isospin pairing, odd-even staggering, nuclear isomers, and the exceptional stability of ^{4}He all emerge from the topology and geometry of composite threefoil knots as structural consequences of the connect-sum construction. The binding-energy fit—two parameters matching Weizsäcker's five on 50 nuclei, with accurate out-of-sample predictions—provides quantitative support for these structural

correspondences. Further analogies with Pauli exclusion, charge quantisation, and sub-nucleon structure are noted as speculative and collected in Appendix A [15,16].

Out-of-sample predictions for ^{244}Pu and ^{252}Cf validate the model beyond its training set, and ropelength calculations for superheavy nuclei up to $Z = 164$ identify topologically favoured configurations that may correspond to the island of stability. The golden-angle packing analysis provides a geometric explanation for the iron peak ($A = 56 \approx F_{10} = 55$) and predicts that $Z = 164$ configurations have the lowest Voronoi defect fraction of any nucleus examined.

The open questions—magic numbers, precise spectroscopy, tunnelling rates—each have a well-defined computational path within the existing framework, requiring no new parameters or postulates. Whether the topological correspondence reflects a deep geometric layer in nuclear structure or a fortuitous coincidence is ultimately an empirical question. The falsifiability tests of Section 10.5 offer a direct path to an answer, and we invite the community to carry them out.

Python 3.11.9 code for all computations is available at Zenodo [17].

Funding: This research received no external funding. The APC was funded by the author.

Data Availability Statement: The Python 3.11.9 code and numerical data supporting the results of this study are openly available on Zenodo at https://zenodo.org/records/18743654 (accessed on 23 February 2026).

Acknowledgments: The conceptual framework presented here—nucleons as threefoil knots, nuclei as their connect-sums, and the use of ropelength as a geometric proxy for soliton binding energy—is the author's own, as are the specific identifications of chirality alternation with isospin pairing, linking number with electric charge, golden-angle packing with shell structure, and the Fibonacci–iron-peak connection. The numerical implementation, data analysis, and manuscript preparation were carried out with substantial assistance from large language models, in particular Claude Sonnet 4.6 (Anthropic) and DeepSeek-V3, which served as computational collaborators: generating and debugging code, performing literature cross-checks, and stress-testing arguments. All scientific claims and interpretations remain the author's responsibility.

Conflicts of Interest: The author declares no conflicts of interest.

Appendix A. Speculative Analogies with Quantum Phenomenology

The correspondences listed here are offered as *speculative analogies*, not as derivations from the ropelength model. They are included because the same geometric framework that correctly predicts nuclear saturation and isospin pairing also possesses structural features consistent with quantum-mechanical phenomena. Whether this consistency is coincidental or reflects genuine physical content requires the falsifiability tests of Section 10.5.

Appendix A.1. Tube Exclusion and Pauli Exclusion

The tube-exclusion constraint in ropelength—two segments of rope cannot occupy the same space—is a geometric consequence of the finite tube thickness, which in turn follows from the $|\psi|^2\psi$ nonlinearity of the underlying field Equation (6). In a linear field theory, superposition holds, and arbitrary numbers of excitations can occupy the same state. In the nonlinear vacuum field, the energy density diverges when two solitons overlap, making co-occupation impossible. This is structurally analogous to Pauli exclusion, applying electively to the topological solitons while leaving linear excitations free to superpose.

Appendix A.2. Reconnection Barriers and Tunnelling

A topological transition in which the knot type changes (e.g., a connect-sum losing a summand, corresponding to nucleon emission) requires the tube to pass through itself. In the field-theory picture, this means the field amplitude must reach zero along a line—a reconnection event with a finite energy barrier. The transition rate is exponentially suppressed, $\Gamma \sim e^{-S_{\text{barrier}}/\hbar}$, analogously to quantum tunnelling and radioactive decay.

Appendix A.3. Discrete Local Minima and Energy Levels

The ropelength functional has discrete local minima, as demonstrated in the isomer analysis of Section 6. The discreteness of this energy landscape is structurally analogous to the discreteness of quantum energy spectra: transitions between minima release energy as radiation, without any quantisation rule being postulated.

Appendix A.4. Odd-Even Staggering

The alternating-chirality connect-sum L–R–L–R–$\cdots$ achieves optimal packing because mirror-image neighbours interdigitate. For even A, every summand has a mirror partner; for odd A, one summand is unpaired, increasing the ropelength. This is structurally analogous to the empirical pairing energy $\delta \approx 12/\sqrt{A}$ MeV.

References

1. Bethe, H.A.; Bacher, R.F. Nuclear physics A. *Rev. Mod. Phys.* **1936**, *8*, 82–229. [CrossRef]
2. von Weizsäcker, C.F. Zur Theorie der Kernmassen. *Z. Phys.* **1935**, *96*, 431–458. [CrossRef]
3. Thomson, W. (Lord Kelvin). On vortex atoms. *Philos. Mag.* **1867**, *34*, 15–24. [CrossRef]
4. Skyrme, T.H.R. A unified field theory of mesons and baryons. *Nucl. Phys.* **1962**, *31*, 556–569. [CrossRef]
5. Faddeev, L.; Niemi, A.J. Stable knot-like structures in classical field theory. *Nature* **1997**, *387*, 58–61. [CrossRef]
6. Cantarella, J.; Kusner, R.B.; Sullivan, J.M. On the minimum ropelength of knots and links. *Invent. Math.* **2002**, *150*, 257–286. [CrossRef]
7. Denne, E.; Diao, Y.; Sullivan, J.M. Quadrisecants give new lower bounds for the ropelength of a knot. *Geom. Topol.* **2006**, *10*, 1–26. [CrossRef]
8. Battye, R.A.; Sutcliffe, P.M. Knots as stable soliton solutions in a three-dimensional classical field theory. *Phys. Rev. Lett.* **1998**, *81*, 4798–4801. [CrossRef]
9. Diao, Y. The additivity of crossing numbers. *J. Knot Theory Ramifications* **2003**, *12*, 857–872. [CrossRef]
10. Pieranski, P. In search of ideal knots. In *Ideal Knots*; World Scientific: Singapore, 1998; Volume 19.
11. Bjorken, J.D. Asymptotic sum rules at infinite momentum. *Phys. Rev.* **1969**, *179*, 1547–1553. [CrossRef]
12. Riedel, T. Protons and neutrons as Borromean-ring solitons in a nonlinear vacuum field. Independent Researcher, 2400 Copenhagen NV, Denmark. 2026, *submitted*.
13. Mackay, A.L. A dense non-crystallographic packing of equal spheres. *Acta Cryst.* **1962**, *15*, 916–918. [CrossRef]
14. Wang, M.; Huang, W.J.; Kondev, F.G.; Audi, G.; Naimi, S. The AME 2020 atomic mass evaluation. *Chin. Phys. C* **2021**, *45*, 030003. [PubMed]
15. Riedel, T. Emergent Maxwell electrodynamics from vacuum phase coherence. Independent Researcher, 2400 Copenhagen NV, Denmark. 2026, *in preparation*.
16. Riedel, T. Atomic electron shells from topological vortex theory. Independent Researcher, 2400 Copenhagen NV, Denmark. 2026, *in preparation*.
17. Riedel, T. Python Code for Composite-Knot Ropelength Calculations. Zenodo, 2026. Available online: https://zenodo.org/records/18743654 (accessed on 23 February 2026).

Disclaimer/Publisher's Note: The statements, opinions and data contained in all publications are solely those of the individual author(s) and contributor(s) and not of MDPI and/or the editor(s). MDPI and/or the editor(s) disclaim responsibility for any injury to people or property resulting from any ideas, methods, instructions or products referred to in the content.